

Charge Order Superstructure with Integer Iron Valence in Fe_2OBO_3

M. Angst,^{1,*} P. Khalifah,² R. P. Hermann,^{3,4} H. J. Xiang,⁵ M.-H. Whangbo,⁵
V. Varadarajan,⁶ J. W. Brill,⁶ B. C. Sales,¹ and D. Mandrus¹

¹Materials Science and Technology Division, Oak Ridge National Laboratory, Oak Ridge, TN 37831, USA

²Department of Chemistry, University of Massachusetts, Amherst, MA 01003, USA

³Institut für Festkörperforschung, Forschungszentrum Jülich GmbH, D-52425 Jülich, Germany

⁴Department of Physics, B5, Université de Liège, B-4000 Sart-Tilman, Belgium

⁵Department of Chemistry, North Carolina State University, Raleigh, NC 27695, USA

⁶Department of Physics and Astronomy, University of Kentucky, Lexington, Kentucky 40506, USA

(Dated: November 13, 2018)

Solution-grown single crystals of Fe_2OBO_3 were characterized by specific heat, Mössbauer spectroscopy, and x-ray diffraction. A peak in the specific heat at 340 K indicates the onset of charge order. Evidence for a doubling of the unit cell at low temperature is presented. Combining structural refinement of diffraction data and Mössbauer spectra, domains with diagonal charge order are established. Bond-valence-sum analysis indicates integer valence states of the Fe ions in the charge ordered phase, suggesting Fe_2OBO_3 is the clearest example of ionic charge order so far.

PACS numbers: 61.50.Ks, 71.30.+h, 71.28.+d, 61.10.Nz

Many physical phenomena in transition metal oxides, including colossal magnetoresistance [1] and high-temperature superconductivity [2], are related to charge ordering (CO). Ideally, CO consists of charge carriers localizing on ions with different integer valences forming an ordered pattern [3]. However, the application of this “ionic CO” concept has been controversial [4, 5], because observed valence separations are usually small, and there is no clear example of CO with integer valences.

Mössbauer spectra on the mixed-valent warwickite Fe_2OBO_3 suggested a large, though not quantified, Fe valence separation below the onset of a monoclinic distortion of the structure (Fig. 1) at 317 K [6]. It is natural then to suspect an ordered arrangement of Fe^{2+} and Fe^{3+} ions (ionic CO), and Fe_2OBO_3 has been suggested as an example of electrostatically driven CO [6]. However, no experimental evidence of a CO superstructure was found on the available polycrystalline samples, and

consequently the occurrence of CO in Fe_2OBO_3 has been under debate [7].

Here, we report the first observation of superstructure reflections in single-crystalline Fe_2OBO_3 , using X-ray diffraction. Combining structural refinement, Mössbauer spectroscopy, and electronic structure calculations, we establish a diagonal CO configuration. Bond-valence-sum analysis indicates that the ordered iron valence states are very close to integer Fe^{2+} and Fe^{3+} . Thus, Fe_2OBO_3 is an excellent example of ionic CO. We discuss implications of the large structural modulations on the relevance of the electron-lattice coupling in driving the CO.

Needle-like single crystals of Fe_2OBO_3 (Fig. 2 inset) with length up to 1.5 cm were grown from a flux with a procedure very similar to the growth of $\text{Fe}_{1.91}\text{V}_{0.09}\text{OBO}_3$ reported by Balaev *et al.* [8], except that we omitted V_2O_3 from the flux to avoid V doping. ^{57}Fe Mössbauer spectra, obtained on powdered crystals using a constant-acceleration spectrometer [9], were similar to previous results [6, 10] with isomer shifts at low T (Fig. 5b) indicating divalent and trivalent Fe with no electron hopping.

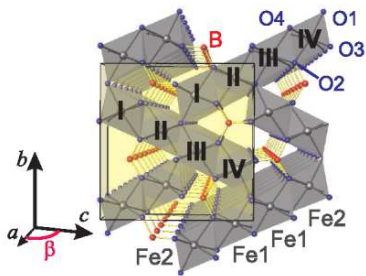


FIG. 1: (Color online) Crystal structure of Fe_2OBO_3 at 355 K. The unit cell (shaded yellow) is orthorhombic ($Pmcn$), at lower T the symmetry is lowered to monoclinic, with a CO superstructure having a $2a \times b \times c$ cell. Structurally distinct Fe_1O_6 and Fe_2O_6 octahedra build ribbons of four edge-sharing chains (numbered, see text) along a . Detail views of the ribbons at 355 and 100 K are given in Fig. 4.

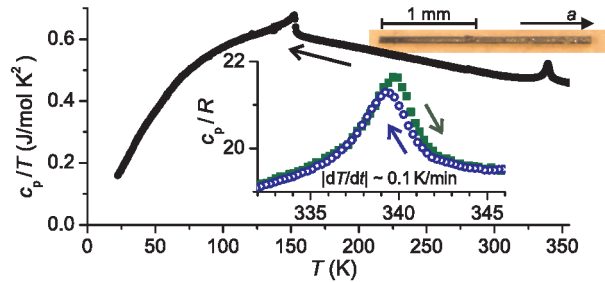


FIG. 2: (Color online) Specific heat c_p/T , measured by ac calorimetry. Lower inset: c_p around 340 K. Upper inset: Fe_2OBO_3 crystal.

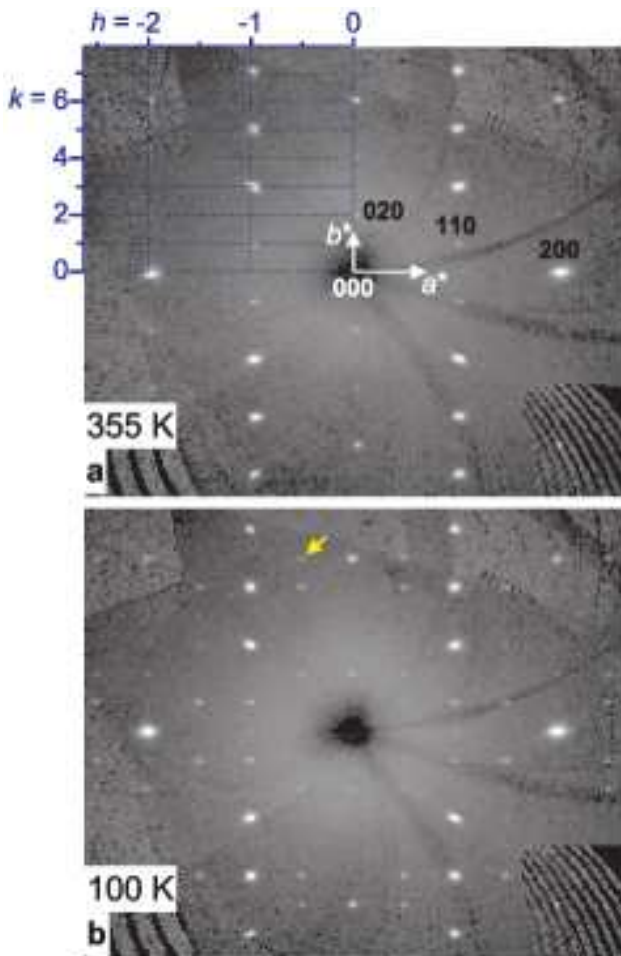


FIG. 3: (Color online) Composite X-ray diffraction precession images with intensities extracted from about 500 individual frames. a: 355 K. Due to an n glide plane, spots with $h + k$ odd are systematically absent. b: 100 K. Weak additional spots (one indicated by an arrow) index to $(h + \frac{1}{2}, k, 0)$, indicating a superstructure with doubled ($2a \times b \times c$) unit cell.

The specific heat (Fig. 2) was measured with ac calorimetry [11] on several crystals giving consistent results. A step-like feature around 153 K is due to the known magnetic transition [12]. A peak at 340 K with ~ 0.25 K hysteresis suggests an additional, weakly first-order, phase transition, which according to a powder diffraction study [13] corresponds to the monoclinic-orthorhombic transition, and which we attribute to the onset of CO. The estimated entropy change associated with the transition is very small ($\sim 0.01 R/\text{Fe ion}$, $R = 8.14 \text{ J/mol/K}$), but we point out that ac calorimetry is sensitive only to the reversible heat flow.

To corroborate the CO, we collected single-crystal X-ray diffraction data with a Bruker SMART APEX CCD diffractometer, using $\text{MoK}\alpha$ radiation. Figure 3 shows composite precession images of the $hk0$ plane with intensities extracted from about 500 individual frames measured at 355 K (a) and 100 K (b). The pattern at 355 K

TABLE I: Refinement results [14] for Fe sites in Fe_2OBO_3 at 355 K (space group $Pm\bar{c}n$, $a = 3.18 \text{ \AA}$, $b = 9.40 \text{ \AA}$, $c = 9.25 \text{ \AA}$) and 100 K (average structure, space group Pc , $2a = 6.33 \text{ \AA}$, $b = 9.38 \text{ \AA}$, $c = 9.25 \text{ \AA}$). Average Fe-O bondlengths, bond-valence-sum, and distortion parameter (see text).

Site	$\langle d(\text{Fe-O}) \rangle / \text{\AA}$	Bond Valence Sum	Distortion Γ
355 K			
Fe1	2.094(2)	2.39(1)	2.8
Fe2	2.088(2)	2.46(1)	4.0
100 K			
Fe1a	2.140(6)	2.04(3)	5.9
Fe2a	2.154(6)	2.03(3)	7.5
Fe1b	2.020(6)	3.02(5)	0.4
Fe2b	2.019(6)	3.07(5)	0.0
Fe1c	2.098(7)	2.35(8)	2.9
Fe2c	2.087(6)	2.47(8)	3.2
Fe1d	2.098(6)	2.34(8)	2.9
Fe2d	2.086(6)	2.48(8)	3.6

is expected for the $Pm\bar{c}n$ (no. 62) space group, and the refined structure (Figs. 1 and 4a [14]) was very similar to the one reported for polycrystalline Fe_2OBO_3 [6]. At 100 K, weak additional spots indexing to $(h + \frac{1}{2}, k, 0)$ indicate a superstructure with $2a \times b \times c$ cell, attributed to CO as detailed below. Visual inspection of the raw data indicated overlapping peaks of roughly equal intensity consistent with monoclinic twinning with similar weight of domains with opposite sense of monoclinic distortion. The twinned peaks were not sufficiently resolved and therefore the refinement was conducted for the combined peaks. As a result, the monoclinic angle β could not be refined, and was set to 90° .

To assess possible symmetries, the data were first refined with no symmetry constraints (space group $P1$). A Pc (No. 7) space group symmetry was apparent, and a corresponding refinement (Fig. 4b) had a residual $R[F^2 > 4\sigma(F^2)] = 4.62\%$ significantly better than alternative space groups [14]. Small (very weak intensity) reflection condition violations and a Flack parameter close to 50% suggest that the structure is not homogeneous, but an average of domains with different, possibly centro-symmetric, structure. Room temperature diffraction data are very similar to the 100 K data, indicating negligible influence of the magnetic transition on the CO.

For octahedrally coordinated Fe^{2+} and Fe^{3+} ions, the expected average Fe-O bondlengths are 2.16 and 2.02 \AA , respectively [15]. For the refined structure, Fe-O bondlengths for half of the eight Fe sites are intermediate and similar as at 355 K (Table I), suggesting CO in only half of the chains. However, M\"ossbauer spectra show that the local structure is different because there is no intermediate valence Fe in the low T phase (Fig. 5b). The refined

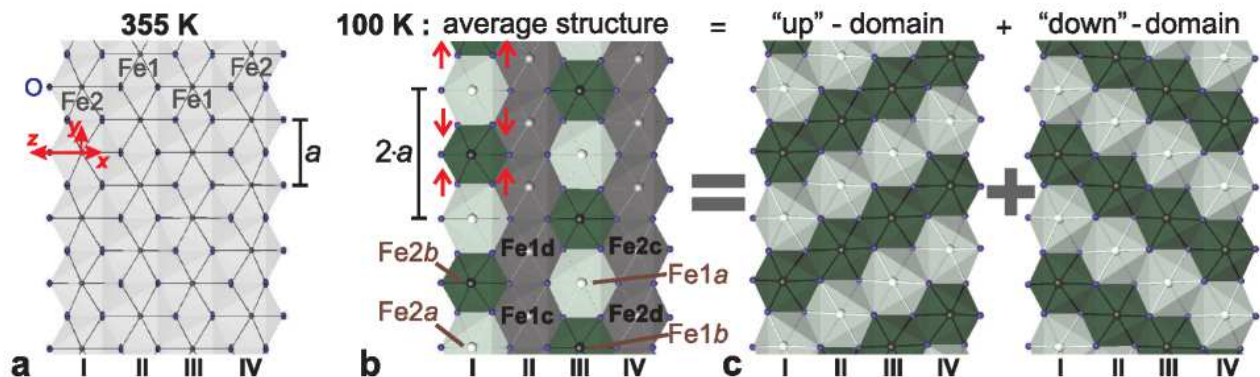


FIG. 4: (Color online) Charge order in the four-chain ribbons (numbered as in Fig. 1). a: 355 K. Atoms are drawn as thermal ellipsoids. For one FeO_6 octahedron a local coordinate system is indicated. b,c: CO at 100 K (high/low valence Fe is shaded dark/bright): The “global” structure, refined in Pc (b) arises from averaging domains with different diagonal order (c). Large oxygen shifts within the superstructure are emphasized by red arrows in b.

structure thus arises from averaging local structures of two types of domains. In two of the chains, II and IV in Fig. 4, structural distortions are averaged out, indicating that these sites have opposite valence, and thus distortions, in the two domain types. The CO in the other two chains is clearly preserved, indicating that their Fe sites have identical valences in all domains. Because the Fe sites with equal a position in the chains with globally preserved CO have opposite valence, the local CO configuration is diagonal, with “up” and “down” diagonals making up the two types of domains (Fig. 4c).

To corroborate the local diagonal CO, we per-

formed first principles electronic structure calculations (GGA+U, with fixed cell, but in contrast to [20] optimized atom positions), using techniques as described in [21]. The GGA+U calculations ($U = 5.5 \text{ eV}$, $J = 0.89 \text{ eV}$ [20]) started with the crystal structure as reported by Attfield *et al.* [6] with doubled a axis, in which all Fe atoms have a uniform valence $\text{Fe}^{2.5+}$. As in [20], a diagonal configuration with charge separation was obtained even with fixed atom positions. Relaxing atom positions led to an additional decrease in energy (total CO gain 174.5 meV/Fe ion), with CO distortions of the optimized atom positions (shown in Fig. 4c) qualitatively equal to the refined ones (neglecting the averaged out sites in chains II and IV), though about 20% less in magnitude.

The shifts in the oxygen positions (Fig. 4b arrows) cause the average Fe-O bondlengths for sites Fe1a and Fe2a to increase and for sites Fe1b and Fe2b to decrease. Valence states and ion sizes are intimately related, allowing the length of the Fe-O bonds to be used to calculate the Fe valence through bond-valence-sum (BVS) analysis [22]. The BVS is

$$V = \sum_i \exp[(d_0 - d_i)/0.37], \quad (1)$$

where V is the valence of an ion to be determined, d_i are the bondlengths to other ions, and d_0 is a tabulated [22] empirical parameter characteristic for a cation-anion pair. At all temperatures the BVS of B and O are close to 3 and -2 , respectively, as expected. A complication for Fe is that the empirical d_0 are slightly different for different valence states. Using tabulated [22] d_0 for both Fe^{2+} -O and Fe^{3+} -O, the calculated valences for ions Fe1a, Fe2a and Fe1b, Fe2b are within 0.2 of 2 and 3, respectively. As is customary in this case [23], the final valences were then calculated using d_0 of Fe^{2+} -O for ions Fe1a and Fe2a and d_0 of Fe^{3+} -O for ions Fe1b and Fe2b. For the averaged sites in chains II, IV at low T and all Fe sites at high T the

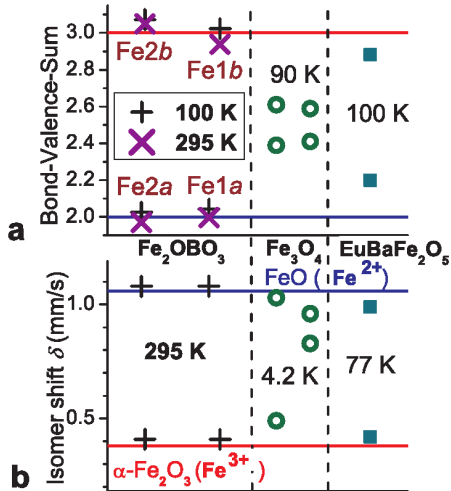


FIG. 5: (Color online) Integer valence separation. a: Fe valence from bond-valence-sum analysis on four sites indicated in Fig. 4b (+), compared to the classical CO example magnetite (B sites, \circ [16]) and the clearer example $\text{EuBaFe}_2\text{O}_5$ (\blacksquare [17]). b: Mössbauer isomer shifts relative to αFe (+), compared to magnetite (B sites, \circ [18]) and $\text{EuBaFe}_2\text{O}_5$ (\blacksquare [17]). The two horizontal lines represent isomer shifts[19] for Fe^{2+} in FeO (blue) and Fe^{3+} in Fe_2O_3 (red) at room temperature.

BVS are intermediate between 2 and 3, and the final valences were obtained by averaging the valences calculated with d_0 for Fe^{2+} and Fe^{3+} .

Averaging over anti-phase domains can only decrease the difference between high and low valence Fe-O bondlengths in the average structure. Consequently the valence separation from BVS obtained from any refined global average structure provides a lower limit for the actual local separation. We focus on the sites in chains I and III, which provide the most stringent limit. These Fe valences are integer within the resolution of the method (Fig. 5a). Fe_2OBO_3 is the first CO oxide for which BVS clearly indicate integer valence for both valence states. The valence separation is considerably larger than in the so far clearest examples, YBaFe_2O_5 [24] and related compounds (~ 0.7), and much larger than in the classical, though not fully understood, CO example magnetite ($\lesssim 0.4$ [16]) or in the colossal magnetoresistance manganites (~ 0.45 [5]). *The large valence separation suggests that Fe_2OBO_3 is an ideal example of ionic charge order.*

In agreement with the large valence difference, Mössbauer spectral isomer shifts δ (Fig. 5b) for two doublets are close to δ of the Fe^{3+} compound Fe_2O_3 and for the other two doublets to δ of the Fe^{2+} compound FeO. The reason that Fe_2OBO_3 is unique among oxides in demonstrating ionic CO may be attributed to an antagonistic inductive effect[25] from the B-O bonds. Since B is more electronegative than Fe, O prefers to share its electrons with B, making the Fe-O bonds more ionic.

The large ($> 0.2 \text{ \AA}$) oxygen shifts along a accompanying the CO also affect the distortions of the coordination octahedra. At high T the largest distortion is an elongation along a (Fig. 4a), leading to a distortion parameter Γ , defined as the difference in % between bondlengths in the local xy plane (Fig. 4a) and those perpendicular to it, of 3 to 4%. In the CO state, this distortion is reduced almost completely for Fe^{3+} sites, but increased for Fe^{2+} sites, consistent with the extra electron occupying a d_{xy} orbital with lobes $\parallel a$. Because the distortion lifts the degeneracy of the t_{2g} orbitals, an energy gain associated with the Jahn-Teller effect [26] likely contributes to the overall energy gain of charge localization and order. Thus, CO in Fe_2OBO_3 is not driven *entirely* by electrostatic interactions between carriers, although the latter alone seems to be sufficient in establishing CO, as indicated by the GGA+U calculations with atom positions fixed. This exemplifies the relevance of electron-lattice effects in correlated oxides, which likely is ubiquitous.

In summary, superstructure reflections at in Fe_2OBO_3 arise from diagonal CO with two domains and Fe valence states very close to integer, suggesting that Fe_2OBO_3 is an ideal example for ionic CO. Magnitude and form of the atomic displacements in the CO suggest that electrostatic energy is not the only relevant energy scale, but coupling to the lattice is important as well. Very anisotropic displacement parameters of the oxygen atoms already at

355 K (Fig. 4a) hint at significant precursor effects to the CO transition; a detailed study of the evolution of the CO with temperature is in progress.

We thank A. Payzant, W. Schweika, A. W. Sleight, B. Chakoumakos, J. Tao, F. Grandjean, O. Swader, and O. Garlea for assistance and discussions. Research at ORNL sponsored by the Division of Materials Sciences and Engineering, Office of Basic Energy Sciences (OS), US Department of Energy (DOE) (contract DE-AC05-00OR22725); at NCSU by OS, DOE (DE-FG02-86ER45259); at UK by NSF (DMR-0400938); at UL: FNRS credit 1.5.064.05.

* email: angst@ornl.gov

- [1] Y.-D. Chuang *et al.*, Science **292**, 1509 (2001); G. C. Milward, M. J. Calderon, and P. B. Littlewood, Nature **433**, 607 (2005).
- [2] D. Reznik *et al.*, Nature **440**, 1170 (2006); T. Valla *et al.*, Science **314**, 1914 (2006).
- [3] E. Wigner, Phys. Rev. **46**, 1002 (1934); E. J. W. Verwey, Nature **144**, 327 (1939).
- [4] M. Coey, Nature **430**, 155 (2004).
- [5] J. García and G. Subías, J. Phys.: Condens. Matter **16**, R145 (2004).
- [6] J. P. Attfield *et al.*, Nature **396**, 655 (1998).
- [7] J. Garcia and G. Subias, Phys. Rev. B **74**, 176401 (2006); I. Leonov *et al.*, *ibid.* **74**, 176402 (2006).
- [8] A. D. Balaev *et al.*, J. Exp. Theor. Phys. **97**, 989 (2003).
- [9] R. P. Hermann *et al.*, Phys. Rev. B **70**, 214425 (2004).
- [10] A. P. Douvalis *et al.*, J. Phys.: Condens. Matter **12**, 177 (2000).
- [11] M. Chung *et al.*, Phys. Rev. B **48**, 9256 (1993).
- [12] M. A. Continentino *et al.*, Phys. Rev. B **64**, 014406 (2001).
- [13] A. Payzant (unpublished).
- [14] Details of the refined structures are deposited in the Inorganic Crystal Structure Database with accession numbers 417971, 417972 (355, 100 K).
- [15] R. D. Shannon, Acta Cryst. A **32**, 751 (1976).
- [16] J. P. Wright, J. P. Attfield, and P. G. Radaelli, Phys. Rev. Lett. **87**, 266401 (2001).
- [17] P. Karen, K. Gustafsson, and J. Lindén, J. Solid State Chem. **180**, 138 (2007).
- [18] F. J. Berry, S. Skinner, and M. F. Thomas, J. Phys.: Condens. Matter **10**, 215 (1998).
- [19] G. Shirane, D. E. Cox, and S. L. Ruby, Phys. Rev. **125**, 1158 (1962).
- [20] I. Leonov *et al.*, Phys. Rev. B **72**, 014407 (2005).
- [21] H. J. Xiang and M.-H. Whangbo, Phys. Rev. Lett. **98**, 246403 (2007).
- [22] I. D. Brown and D. Altermatt, Acta Cryst. B **41**, 244 (1985); N. E. Brese and M. O’Keeffe, *ibid.* **47**, 192 (1991).
- [23] See, e.g., J. Rodriguez-Carvajal *et al.*, Phys. Rev. Lett. **81**, 4660 (1998).
- [24] P. M. Woodward and P. Karen, Inorg. Chem. **42**, 1121 (2003).
- [25] F. Menil, J. Phys. Chem. Solids **46**, 763 (1985).
- [26] H. A. Jahn and E. Teller, Proc. R. Soc. Lond. A **161**, 220 (1937).